Available online at www.sciencedirect.com
ScienceDirect
Journal of Nuclear Materials 361 (2007) 52–61
journal of nuclear materials
www.elsevier.com/locate/jnucmat

Computer simulation of the interaction of carbon atoms with self-interstitial clusters in α-iron

K. Tapasa [a], A.V. Barashev [a,*], D.J. Bacon [a], Yu.N. Osetsky [b]

[a] Department of Engineering, The University of Liverpool, Brownlow Hill, Liverpool L69 3GH, UK
[b] Computer Science and Mathematics Division, ORNL, Oak Ridge, TN 37831-6138, USA

Received 27 July 2006; accepted 19 October 2006

Abstract

Static and dynamic properties of clusters of self-interstitial atoms and their complexes with carbon (C) atoms in α-iron are studied by molecular dynamics method using a pairwise interatomic potential for iron–carbon interaction and a many-body potential for iron. The effect of C atoms on the configuration, stability and migration of $\frac{1}{2}\langle 1\,1\,1\rangle$, $\frac{1}{2}\langle 1\,1\,0\rangle$ and $\langle 1\,0\,0\rangle$ interstitial clusters is investigated. In the framework of the simple model of interstitial solute used here, C atoms enhance the relative stability of $\langle 1\,0\,0\rangle$ over $\frac{1}{2}\langle 1\,1\,1\rangle$ clusters, but not enough to explain their common occurrence under irradiation. Clusters of seven interstitials or smaller are able to co-migrate with C atoms with a reduced mobility compared with pure iron. Bigger clusters have dislocation structure and are immobilised: C migrates along the core of their periphery as in the core of a straight edge dislocation. C dissociates from all clusters at high enough temperature.

PACS: 61.80.Az; 61.82.Bg

1. Introduction

It is known from experiment that interaction of interstitial carbon (C) atoms with lattice defects affects mechanical properties of ferritic steels, such as their strength [1], properties of single vacancies and interstitial atoms [2], and microstructure development under irradiation conditions [3,4]. Understanding of the latter process is still poor, even in pure iron (Fe), where for example, the occurrence of interstitial-type loops with the Burgers vector $\boldsymbol{b} = \langle 1\,0\,0\rangle$ [5,6] remains unexplained. Eyre and Bullough [7] proposed that a $\langle 1\,0\,0\rangle$ loop can form as a result of $\frac{1}{2}\langle 1\,\bar{1}\,0\rangle$ shear of a faulted $\frac{1}{2}\langle 1\,1\,0\rangle$ loop. However, calculations with existing empirical interatomic potentials for α-Fe do not provide support for this reaction, for $\frac{1}{2}\langle 1\,1\,1\rangle$ loops are found to be the most stable. Furthermore, molecular dynamics (MD) simulations of displacement cascades predict that only $\frac{1}{2}\langle 1\,1\,1\rangle$ clusters of self-interstitial atoms (SIAs) are produced in Fe under irradiation with energetic particles [8]. Finally, although it is observed by MD that segments of $\langle 1\,0\,0\rangle$ type are formed as a result of the interaction between two mobile $\frac{1}{2}\langle 1\,1\,1\rangle$ clusters [9,10], these are dynamically unstable and a single $\frac{1}{2}\langle 1\,1\,1\rangle$ dislocation loop eventually forms.

* Corresponding author.
E-mail address: a.barashev@liv.ac.uk (A.V. Barashev).

0022-3115/$ - see front matter © 2006 Elsevier B.V. All rights reserved.
doi:10.1016/j.jnucmat.2006.10.022

One of the reasons for these results may be an incorrect description of the relative stability of single SIAs of different configuration. MD studies mentioned above used a many-body interactomic potential of Finnis–Sinclair-type (F–S) due to Ackland et al. [11], which gives the formation energy of the $\langle 1\,1\,0\rangle$ dumbbell to be only 0.13 eV lower than that of a $\langle 1\,1\,1\rangle$ crowdion. With the embedded-atom-method-type (EAM) potential proposed recently [12], this difference is ~0.5 eV and hence closer to the value 0.7 eV obtained by *ab initio* calculations based on the density-functional theory (DFT) [13]. Furthermore, the $\langle 1\,1\,0\rangle$ configuration is more stable with respect to the $\langle 1\,1\,1\rangle$ for clusters of up to four SIAs with this newer potential [13], which is why we use it here.

Another possibility is that interstitial impurities, such as carbon, may affect relative stability of different SIA clusters. However, development of interatomic potentials for the Fe–C system required for study of stability has lagged behind those for α-Fe with substitutional solutes, and only a few Fe–C potentials have been proposed to date. Johnson et al. [14] developed a pairwise potential for Fe–C for use with a pair potential for Fe by fitting to the experimental value of 0.86 eV for the migration energy of a C interstitial [15], zero activation volume of migration [16] and a vacancy-C binding energy of 0.41 eV [17]. C–C interaction was not considered in this model. This potential reproduces satisfactorily the experimental value of the energy of solution of a C atom in α-Fe relative to that in Fe_3C [18], and gives the octahedral site as the most stable one for the C interstitial and the tetrahedral site as the saddle-point for C jump from one octahedral site to another, which is consistent with experiment [19] and DFT calculations [20]. Although the volume expansion due to a C atom is $\sim 0.3\Omega$, where Ω is the Fe atomic volume, compared with $\sim 0.8\Omega$ deduced from the experimental value of lattice parameter change with C composition [21], the relaxation of Fe atoms neighbouring a C atom obtained in Ref. [22] by a combination of the Fe–C potential of Johnson et al. and the EAM-type potential of Ackland et al. [12] is in good agreement with that found from a recent *ab initio* calculation by Domain et al. [20].

With regard to other Fe–C potentials in the literature, the rescaled version of the potential of Johnson et al. proposed by Rosato [23] for use with a F–S-type potential for Fe yields 1.14 eV for the C migration energy, which is much too high. An EAM-type potential fitted to *ab initio* data on metastable carbide FeC with B1 structure developed by Ruda et al. [24] gives the tetrahedral site as the most stable position for a C atom, which is in contradiction with experiment and *ab initio* results. Lee [25] has developed very recently a modified EAM potential for Fe–C. It produces a C–V binding energy of 0.9 eV, which is close to the value 0.85 eV deduced from experiment by Vehanen et al. [2], but much higher than the values 0.41, 0.47 and 0.51 eV obtained from experiment by Arndt and Damask [17], *ab initio* calculation by Domain et al. [20] and the potentials used here (see [22]), respectively.

Another unresolved problem in understanding and describing C interaction with point defects concerns the sign of the interaction energy with self-interstitial atoms (SIAs). For example, the DFT calculations of Domain et al. [20] show repulsion between a C atom and a single SIA in $\langle 1\,1\,0\rangle$ dumbbell configuration for the largest model considered (128-atom cell), with a binding energy of −0.19 eV in nearest neighbour coordination (distance $a_0/2$, where a_0 is the lattice parameter) and −0.31 and −0.09 eV for the two C–SIA pairs with second-neighbour spacing $(a_0/\sqrt{2})$. (These three arrangements are labelled 1, 2 and 3 in Fig. 13 of [20].) In contrast, experiments offer evidence that SIAs are immobilised by C atoms at low enough temperature and the recovery stage I_E in Fe–C solutions is attributed to dissociation of SIA–C complexes, the binding energy of which is estimated to be ~0.1 eV [2,26]. The potential set used here gives 0.58, −0.10 and 0.31 eV for the three C–SIA pairs 1, 2 and 3 in [20] and the EAM potential of Lee [25] results in 0.68 eV for pair 1. In addition, the formation of carbon atmospheres around dislocations [1] implies existence of strong binding between these defects. The corresponding binding energy is estimated in the framework of elasticity theory to be equal to 0.70 eV [27], which is consistent with the value of 0.75 eV [28] calculated using the Fe–C potential set of Johnson et al. [14].

Clearly, there are several anomalies between atomic-level simulation, *ab initio* calculation and experiment that are not yet resolved. All empirical potentials proposed to date have some deficiencies. As far as the relative stability of SIAs and their clusters is concerned, the EAM potential of Ackland et al. [12] for Fe–Fe interaction currently provides the best description. For dilute Fe–C solid solution, the Fe–C potential of Johnson et al. [14] remains a good choice, and so we have used a combination

of these potentials for the present work. A complete account of the effect of carbon and point defect properties is presented in a separate paper [22].

For the present work, atomic-scale computer simulation has been applied to study the effect of C atoms on the configuration and migration of $\frac{1}{2}\langle 1\,1\,1\rangle$, $\frac{1}{2}\langle 1\,1\,0\rangle$ and $\langle 1\,0\,0\rangle$ SIA clusters. Migration of carbon in the core of the periphery of clusters has also been analysed. The paper is organised as follows. The calculation methods are described in Section 2 and the properties of different types of SIA cluster in pure iron and their interaction with C atoms at 0 K are presented in Section 3. Results of MD simulation of the motion of SIA clusters in the presence of C solute and the motion of C in the core of interstitial loops are presented in Section 4. The conclusions are drawn in Section 5.

2. Calculation model

Two atomic-scale simulation techniques were applied. Molecular statics relaxation was employed via a combination of conjugate gradients potential energy minimisation and quasi-dynamic quenching to study defect configurations at temperature $T = 0$ K and to calculate formation, binding and migration energy. MD was used to model configurations at $T > 0$ K and provide data for thermally activated motion of defects. In both cases the calculations were performed using periodic boundary conditions at constant volume. The shape and size of the simulation box depended on the type and particular property of defects under consideration. The MD calculations were performed by adjusting the lattice parameter, a_0, for zero pressure conditions. The integration of equations of motion was performed using the velocity Verlet-leapfrog algorithm [29] with variable time step, which was controlled by fixing the maximum displacement of the fastest atom at each step to be equal to $0.005a_0$. The mean time step was from 0.6 to 0.8 fs depending on the temperature.

SIA clusters with Burgers vector $\boldsymbol{b} = \frac{1}{2}\langle 1\,1\,1\rangle$, $\frac{1}{2}\langle 1\,1\,0\rangle$ and $\langle 1\,0\,0\rangle$ were studied. (We use the term Burgers vector throughout, although small clusters of a few SIAs do not develop full dislocation character.) Clusters were formed by creating closely packed dumbbells of appropriate orientation in a perfect crystal and then relaxing to minimise the potential energy. $\frac{1}{2}\langle 1\,1\,0\rangle$ and $\langle 1\,0\,0\rangle$ clusters have habit planes perpendicular to their Burgers vectors, i.e. $\{1\,1\,0\}$ and $\{1\,0\,0\}$, respectively. The habit plane of $\frac{1}{2}\langle 1\,1\,1\rangle$ SIA clusters was found to depend on cluster size, being $\{1\,1\,1\}$ for clusters of less than about seven SIAs and tending towards $\{1\,1\,0\}$ for larger clusters. In most calculations, the cluster shape was the closest to that of the most stable configuration, i.e. hexagon or rhombus for $\frac{1}{2}\langle 1\,1\,1\rangle$, rhombus for $\frac{1}{2}\langle 1\,1\,0\rangle$ and square for $\langle 1\,0\,0\rangle$ clusters. These correspond to loop sides oriented along closely packed directions.

3. Results of static simulations

3.1. Configuration and formation energy of SIA clusters

The static relaxations were performed in a simulation box with axes along $\langle 1\,0\,0\rangle$ directions and size $(20a_0)^3$. Generally, $\frac{1}{2}\langle 1\,1\,1\rangle$ and $\frac{1}{2}\langle 1\,1\,0\rangle$ clusters were observed to have regular shape with corresponding Burgers vectors clearly identifiable. Small $\langle 1\,0\,0\rangle$-type clusters of two to five SIAs have distorted configurations with individual SIAs tilted into different directions. The most interesting observation is that $\frac{1}{2}\langle 1\,1\,0\rangle$ clusters larger than seven SIAs do indeed have a tendency to shear to $\langle 1\,0\,0\rangle$ configuration, as predicted by Eyre and Bullough [7].

Fig. 1(a) and (b) presents two examples of the relaxed configuration of clusters of nine and 25 SIAs initially in $\frac{1}{2}\langle 1\,1\,0\rangle$ type configuration. A slice of three (0 0 1) atomic planes through the middle of the cluster is shown, with the light spheres indicating positions of pairs of atoms that formed the initial $[1\,\bar{1}\,0]$ dumbbell interstitials. The dislocation core of the cluster perimeter is indicated in the figures and a Burgers circuit is plotted in each case. This shows that the small cluster in Fig. 1(a) remains a $\boldsymbol{b} = \frac{1}{2}[1\,\bar{1}\,0]$ defect, albeit with a small $[1\,1\,0](\bar{1}\,1\,0)$ shear across the cluster plane. The shear displacement is $\frac{1}{2}[1\,1\,0]$ for the larger cluster in Fig. 1(b), so that $\boldsymbol{b}$ has transformed to $\langle 1\,0\,0\rangle$ type by the process $\frac{1}{2}[1\,\bar{1}\,0] + \frac{1}{2}[1\,1\,0] = [1\,0\,0]$. The location of the edge dislocation symbols shows that the loop has rotated on its glide prism away from the $(1\,\bar{1}\,0)$ orientation. Thus, static simulations suggest that $\frac{1}{2}\langle 1\,1\,0\rangle$ SIA clusters of about 16 SIAs and larger may transform into $\langle 1\,0\,0\rangle$ configuration. This possibility is verified by MD in the next section.

Fig. 2 shows the binding energy of SIA clusters, normalised by the number of SIAs, as a function of cluster size. The reference state is a set of isolated SIAs in $\langle 1\,1\,0\rangle$ dumbbell configuration, each with the formation energy of 3.53 eV. It is seen that for clusters containing four SIAs or fewer, the most

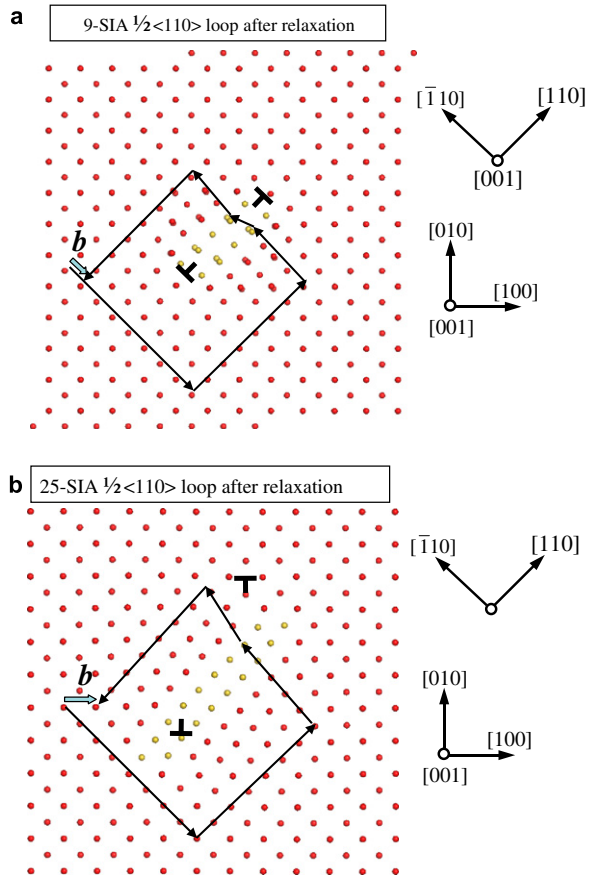

Fig. 1. Relaxed configuration of (a) 9- and (b) 25-SIA clusters initially in $\frac{1}{2}\langle 1\,1\,0\rangle$ configuration. A slice of three (0 0 1) atomic planes through the middle of the cluster is shown. The Burgers circuit construction used to define $\boldsymbol{b}$ is shown and the position of the loop core is indicated by the edge dislocation symbols.

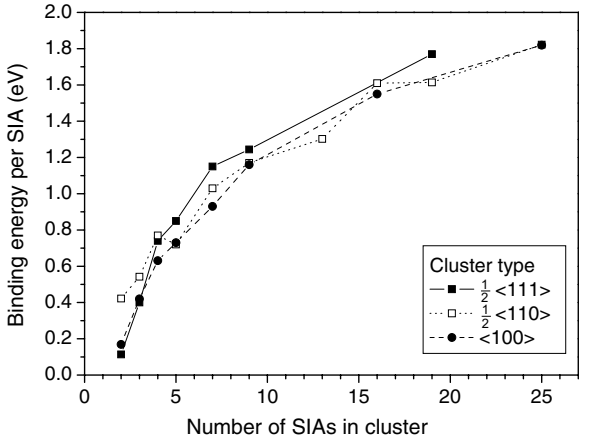

Fig. 2. Binding energy per SIA of interstitial clusters as a function of cluster size.

stable configuration is a set of $\langle 1\,1\,0\rangle$ dumbbells, while the arrangement of crowdions in $\langle 1\,1\,1\rangle$ configuration is preferable for bigger clusters. Some results on the formation and binding energy of the clusters (for which the interaction with C atoms was also studied) are collected in Table 1. The formation energy values for the 4-SIA clusters in Fe are close to those given by Willaime et al. [13] using the same potential.

3.2. Interaction of SIA clusters with C atoms

Carbon atoms were introduced near clusters of the three principal types consisting of four, seven, nine, 16 and 19 SIAs. The simulation boxes were of cuboid shape elongated along the direction of the cluster Burgers vector. For $\langle 1\,0\,0\rangle$ clusters, a cubic box was used with axes along $\langle 1\,0\,0\rangle$ directions and box size $(20a_0)^3$. For $\frac{1}{2}\langle 1\,1\,1\rangle$ and $\frac{1}{2}\langle 1\,1\,0\rangle$ clusters, a box with [1 1 1], [1 1 $\bar{2}$] and [1 $\bar{1}$ 0] axes was used, elongated along the direction of the Burgers vector and of size up to $23\sqrt{3}\times 5\sqrt{6}\times 10\sqrt{2}(a_0)^3$ and $12\sqrt{3}\times 9\sqrt{6}\times 15\sqrt{2}(a_0)^3$, respectively. One or two carbon atoms were placed in all possible sites in the vicinity of a cluster and the binding energy was computed after atomic relaxation. (Note that C–C interaction is not treated in our model, so when the effect of two C atoms was considered, one was placed in the site of maximum attraction to the SIA cluster and the other was placed in the equivalent site on the opposite side of the cluster.)

Results for the formation and binding energy for each cluster are given in Table 1, together with the binding energy of the C–SIA cluster complexes. For the latter energy the reference state is a set of isolated SIAs in $\langle 1\,1\,0\rangle$ dumbbell configuration and isolated C atoms. (For large clusters of 16 and 19 SIAs, it was not possible to ensure that all possible positions of the C atom were considered by static simulation and we cannot be certain that the energy in the table is the maximum binding energy.) In our simulations the $\frac{1}{2}\langle 1\,1\,0\rangle$ clusters of seven and nine SIAs with one C atom relaxed into $\frac{1}{2}\langle 1\,1\,1\rangle$ configuration, but those with two C atoms did not.

Fig. 3 shows two examples of how the binding energy of a C atom with $\frac{1}{2}\langle 1\,1\,1\rangle$ and $\langle 1\,0\,0\rangle$ clusters of nine SIAs depends on the position of the C atom. The values of the energy when the C atom is placed near the cluster are shown in the atomic projections of the Fe interstitials in Fig. 3(a) and (b), and the variation of energy with distance from the habit plane along the rows labelled A and B is shown in

Table 1
Energy (in eV) of SIA clusters with and without C atoms

	Cluster type	Number of SIAs in cluster				
		4	7	9	16	19
Formation energy of cluster	$\frac{1}{2}\langle 1\,1\,1\rangle$	11.18	16.70	20.62	–	33.43
	$\frac{1}{2}\langle 1\,1\,0\rangle$	11.03	17.53	21.97	34.79	–
	$\langle 1\,0\,0\rangle$	11.84	18.50	21.58	31.74	–
Binding energy of cluster	$\frac{1}{2}\langle 1\,1\,1\rangle$	2.94	8.02	11.16	–	33.67
	$\frac{1}{2}\langle 1\,1\,0\rangle$	3.09	7.20	9.83	21.71	–
	$\langle 1\,0\,0\rangle$	2.28	6.22	10.20	24.76	–
Max binding energy of C with cluster	$\frac{1}{2}\langle 1\,1\,1\rangle$	0.86	0.74	0.66	–	0.42
	$\frac{1}{2}\langle 1\,1\,0\rangle$	0.72	–[a]	–[a]	2.04	–
	$\langle 1\,0\,0\rangle$	–	–	1.22	1.13	–
Binding energy of C-cluster complex	$\frac{1}{2}\langle 1\,1\,1\rangle$	3.80	8.76	11.82	–	34.09
	$\frac{1}{2}\langle 1\,1\,0\rangle$	3.81	–[a]	–[a]	23.75	–
	$\langle 1\,0\,0\rangle$	–	–	11.42	25.89	–
Binding energy of 2C atoms with cluster	$\frac{1}{2}\langle 1\,1\,1\rangle$	1.96	1.13	0.76	–	–
	$\frac{1}{2}\langle 1\,1\,0\rangle$	–	–	1.56	2.04	–
	$\langle 1\,0\,0\rangle$	–	–	2.32	2.03	–
Binding energy of 2C-cluster complex	$\frac{1}{2}\langle 1\,1\,1\rangle$	4.90	9.15	11.92	–	–
	$\frac{1}{2}\langle 1\,1\,0\rangle$	–	–	11.39	23.75	–
	$\langle 1\,0\,0\rangle$	–	–	12.52	26.79	–

[a] Relaxed configuration was $\frac{1}{2}\langle 1\,1\,1\rangle$ cluster.

Fig. 3(c). The maximum binding energy was found to be 0.86 and 1.22 eV for $\frac{1}{2}\langle 1\,1\,1\rangle$ and $\langle 1\,0\,0\rangle$ clusters, respectively. It is a general observation that the most stable position for a C atom is near the periphery of a cluster, but the binding energy for other sites, both inside and outside the cluster perimeter, is also high. The distance dependence of the binding energy is not symmetric for the $\langle 1\,1\,1\rangle$ defect because of the threefold stacking sequence of the $\{1\,1\,1\}$ planes.

We note the following interesting observation in Table 1. Consider 9-SIA clusters. The $\frac{1}{2}\langle 1\,1\,1\rangle$ and $\frac{1}{2}\langle 1\,1\,0\rangle$ clusters exhibit the highest and lowest value of the total binding energy in pure iron, respectively, with the $\langle 1\,0\,0\rangle$ defect in-between. The difference between $\frac{1}{2}\langle 1\,1\,1\rangle$ and $\langle 1\,0\,0\rangle$ is 0.96 eV. With the addition of one C atom, the difference between the binding energies reduces to 0.38 eV. (The $\frac{1}{2}\langle 1\,1\,0\rangle$ defect relaxed to the $\frac{1}{2}\langle 1\,1\,1\rangle$ configuration during the simulation.) With two extra C atoms, this difference is -0.60 eV and hence the $\langle 1\,0\,0\rangle$ configuration becomes more stable. Thus, static simulations predict that the $\langle 1\,0\,0\rangle$ configuration can be the most stable if a sufficient number of C atoms is added. The possibility of stabilising the $\langle 1\,0\,0\rangle$ cluster by C atoms is verified by MD in the next section.

4. Results of MD simulations

4.1. Influence of C atoms on dynamic stability of SIA clusters

MD calculations were performed for clusters of various sizes in the range from four to 19 SIAs at temperatures of 300–1200 K. The shape and size of simulation boxes were the same as in the static simulations (see Section 3.2). The initial atomic configurations were obtained by static relaxation prior to imposition of kinetic energy to each atom appropriate to the desired temperature. The simulation time varied from 1 to 19 ns. The following behaviour was observed.

In pure iron, all clusters larger than seven SIAs transform quickly into $\frac{1}{2}\langle 1\,1\,1\rangle$ configuration and migrate one-dimensionally (1-D) along their crowdion axis direction. The 4- and 5-SIA clusters, for which the energy difference between $\frac{1}{2}\langle 1\,1\,1\rangle$ and $\frac{1}{2}\langle 1\,1\,0\rangle$ forms is small, occasionally change their axis between equivalent $\langle 1\,1\,1\rangle$ directions. This rotation of the crowdions occurred only a few times during a simulation, the frequency apparently increasing with temperature. When a carbon interstitial is present, the behaviour is different.

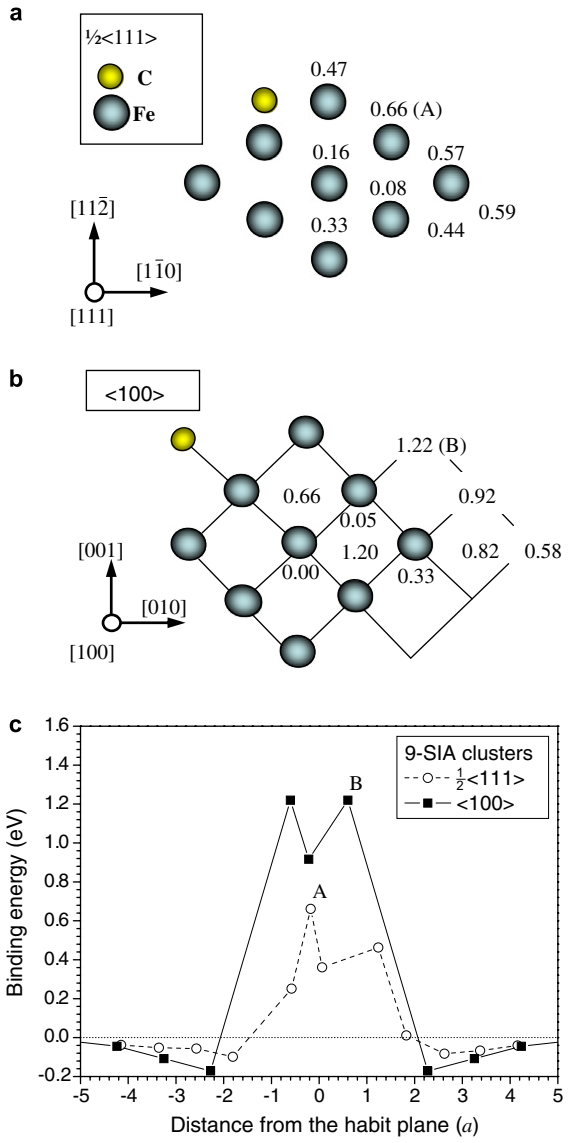

Fig. 3. The binding energy of one C atom in various sites near (a) $\frac{1}{2}\langle 1\,1\,1\rangle$ and (b) $\langle 1\,0\,0\rangle$ clusters of nine SIAs. The Fe interstitials are shown in habit-plane projection and a C atom is depicted in one of the positions of maximum binding energy. (c) The variation of binding energy with distance perpendicular to the habit plane along rows A and B shown in (a) and (b).

A 4-SIA cluster initially created in $\frac{1}{2}\langle 1\,1\,1\rangle$ configuration co-migrates with a C atom. It does not have clear $\frac{1}{2}\langle 1\,1\,1\rangle$ or $\frac{1}{2}\langle 1\,1\,0\rangle$ configuration because the energy difference between these two configurations is reduced further in the presence of a C atom (see Table 1). The migration is significantly slower than in pure iron, for it is controlled by the frequency of C atom jumps in the direction of the cluster axis. For the 5-SIA cluster with one C atom at 900 K, however, we observed formation and survival of the immobile configuration shown in Fig. 4(a) for the period of simulation. In this figure, all individual SIAs are in $\langle 1\,1\,0\rangle$ dumbbell configuration.

A 7-SIA cluster initially created in $\frac{1}{2}\langle 1\,1\,1\rangle$ configuration with one or two C atoms was essentially immobilised at 300 K. It co-migrated with C atoms at 600 and 900 K, and dissociated from them and hence diffused at 1200 K. Co-migration of a C atom along the $\langle 1\,1\,1\rangle$ cluster axis was achieved by jumps both around the perimeter of the cluster and, occasionally, through sites inside it. Accurate statistical analysis of migration of the cluster-C complex was not possible because of the low statistics of jumps. However, it is clear that the cluster jump frequency, i.e. the frequency with which its centre of gravity is displaced by $\frac{1}{2}\langle 1\,1\,1\rangle$ steps, was significantly reduced by the presence of a carbon atom.

The 19-SIA cluster exhibited no mobility when a carbon atom was trapped at the periphery of the cluster, except at 1200 K when dissociation occurred. The cluster retained $\frac{1}{2}\langle 1\,1\,1\rangle$ configuration

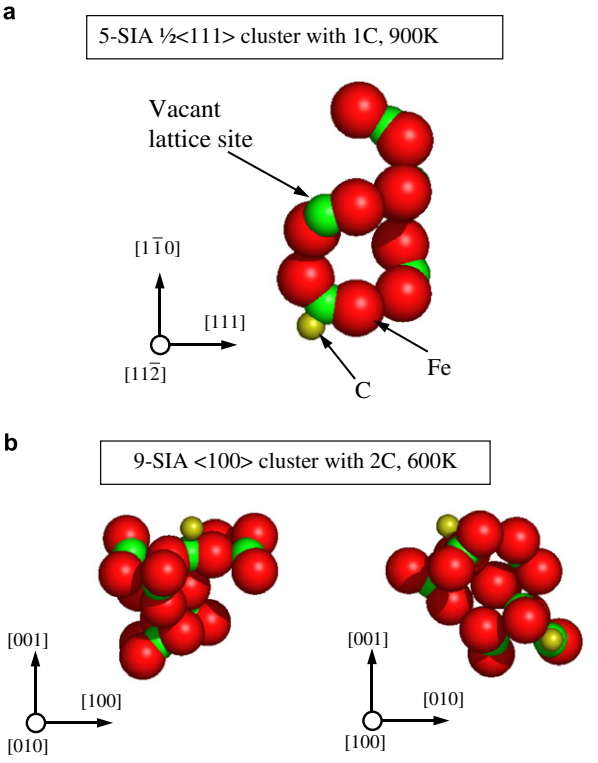

Fig. 4. Configuration formed by (a) the $\frac{1}{2}\langle 1\,1\,1\rangle$ 5-SIA cluster with one C atom at 900 K and (b) the $\langle 1\,0\,0\rangle$ 9-SIA cluster with two C atoms at 600 K.

and goes back and forth around the position of the C atom.

Most of the clusters initially in $\frac{1}{2}\langle 1\,1\,0\rangle$ and $\langle 1\,0\,0\rangle$ configurations with one or two C atoms were found to transform quickly into a $\frac{1}{2}\langle 1\,1\,1\rangle$ configuration. Hence, the presence of C atoms was unable to stabilise these clusters against transformation to this form. Some effect of C was observed in individual cases, however. For example, at 600 K two C atoms formed a sessile complex with a 9-SIA cluster (initially in $\langle 1\,0\,0\rangle$ configuration) shown in Fig. 4(b), whose lifetime extended to the end of the simulation, and delayed the conversion of a 16-SIA $\langle 1\,0\,0\rangle$ cluster into a $\langle 1\,1\,1\rangle$ configuration for ~0.9 ns.

In summary, the dynamic behaviour of clusters containing more than four SIAs in pure Fe simulated with the EAM-type potential of Ackland et al. [12] is similar to that reported previously [30–32] with the F–S-type potential of [11]. In particular, independently of the starting configuration, the clusters transform into $\frac{1}{2}\langle 1\,1\,1\rangle$ configuration. In Fe–C solution, C atoms may immobilize clusters containing a few SIAs for the period of simulation time. Two C atoms may delay transformation of $\langle 1\,0\,0\rangle$ loops or even form a sessile configuration. However, the present MD simulations do not provide evidence for transformation of either $\frac{1}{2}\langle 1\,1\,1\rangle$ or $\frac{1}{2}\langle 1\,1\,0\rangle$ clusters into $\langle 1\,0\,0\rangle$ defects. The main effect of C atoms on SIA clusters is thus seen in the reduction of their mobility, which is controlled by C atom jumps within the core of the cluster perimeter. This is considered next.

4.2. Core migration of C atoms around SIA clusters

For this study, MD simulations of hexagonal clusters of 19, 37 or 61 $\langle 1\,1\,1\rangle$ crowdions with one carbon atom trapped at the perimeter were undertaken. Times of up to 29 ns were simulated at temperatures of 600 to 1200 K. As noted above, the 7-SIA hexagonal cluster was able to migrate along its $\langle 1\,1\,1\rangle$ crowdion axis when a carbon atom was present. The larger clusters considered in this section were not mobile, except when dissociation of the interstitial solute from the cluster occurred at 1200 K. Despite the immobilisation of clusters by carbon at the other temperatures, motion of the interstitial solute in the cluster periphery was observed and is analysed here.

The model hexagonal cluster has sides lying in $\langle 1\,1\,2\rangle$ directions and a glide prism with $\{1\,1\,0\}$ faces of the $[1\,1\,1]$ zone axis. The crystallography for the $[1\,1\,1]$ defect is shown schematically in Fig. 5. As described in detail elsewhere [33], it has characteristics of a small dislocation loop with perfect Burgers vector $\boldsymbol{b} = \frac{1}{2}[1\,1\,1]$. The C atom was found to migrate around the periphery of the cluster for the entire simulation time.

Two kinds of C jump could be distinguished. The majority involved the C atom moving back and forth in the core region of a cluster side. Interestingly, the direction of motion was neither the $[1\,1\,1]$ direction of the prism axis, nor the $\langle 1\,1\,2\rangle$ direction of a loop side nor a $\langle 1\,0\,0\rangle$ direction to the nearest octahedral site, as occurs in Fe far from a cluster. It was found to be the $\langle 1\,1\,1\rangle$ direction lying in a $\{1\,1\,0\}$ face of the glide prism at 70.5° to $[1\,1\,1]$. The jump directions are shown for two of the glide prism faces in Fig. 5. The step vector was $\pm\frac{1}{4}\langle 1\,1\,1\rangle$ with projected length along the cluster side equal to the distance $a_0/\sqrt{6}$ between $\{1\,1\,2\}$ atomic planes. We denote these as A-type jumps. They are the same as those that have been found by computer simulation to occur in the core of a straight $\frac{1}{2}\langle 1\,1\,1\rangle\{1\,1\,0\}$ edge dislocation in Fe and are described in detail in [34]. The other jumps occurred less frequently and took the C atom around a vertex of the cluster to an adjacent side: we denote these as B jumps. The frequency of these jumps was of the order of 10 and 1 ns^{-1} for A and B, respectively, and rather insensitive to cluster size. MD simulation timescale imposes restrictions on their statistical

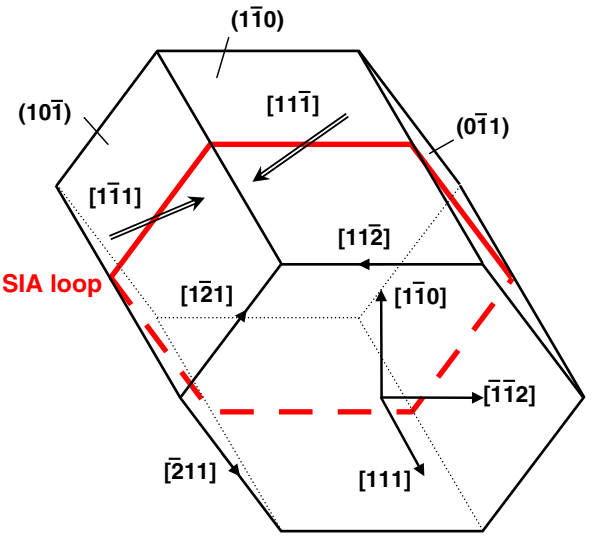

Fig. 5. Schematic illustration of the crystallography of an SIA loop with $\boldsymbol{b} = \frac{1}{2}\langle 1\,1\,1\rangle$ and $\{1\,1\,0\}$ glide prism in iron.

Table 2
Summary of the properties of C jumps around SIA clusters

Cluster size	T (K)	Time (ns)	No. of C jumps		Jump frequency (s^{-1})	
			A	B	A	B
19 SIAs	600	28.70	224	20	7.80	0.70
	800	16.30	141	49	8.65	3.00
	900	17.54	143	45	11.80[a]	3.71[a]
37 SIAs	600	19.26	166	17	8.62	0.88
	900[b]	14.87	178	40	11.97	2.69
61 SIAs	600	10.41	92	1	8.84	0.10
	900	6.20	104	9	16.78	1.45

[a] Averaged values as several C-cluster complex dissociation events occurred during simulation.
[b] A few C-cluster complex dissociation events occurred, but it took very short time for each event (less than 0.25 ns).

analysis. For example, we observed between 92 and 224 A-type jumps (for the 61-SIA and 19-SIA clusters, respectively, at 600 K), but only 9 and 45 B-jumps (for the 61-SIA and 19-SIA clusters, respectively, at 900 K). The jump data are summarised in Table 2 and presented as Arrhenius plots in Fig. 6.

Fig. 6 contains three additional plots for the purposes of comparison. One uses data obtained from MD simulation of C diffusion in pure Fe using the same interatomic potential model as here (open circles) [22]. The second uses frequencies extracted from experimental data on the diffusion coefficient of C in the bulk of α-Fe (dashed line) [35,36]. The third shows frequencies for A-type jumps of C in the core of a straight $\frac{1}{2}\langle 1\,1\,1\rangle\{1\,1\,0\}$ edge dislocation in Fe obtained by simulation by [34], again using the same model potential as in the present work. The values for the dislocation core jumps are higher than those in the bulk by three orders of magnitude at 600 K and an order of magnitude at 900 K. The activation energy in the Arrhenius relationship between the jump frequency and temperature obtained from the straight-fit line shown in Fig. 6 is 0.1 eV for the cluster of 61 SIAs. This is much lower than the value of 0.7 eV for bulk diffusion in the same MD model. Taking into account the limited statistics inherent in our calculations, we conclude that this activation energy for jumps along the side of a cluster compares well with the value of 0.2 eV for those in the core of an infinite straight edge dislocation [34]. It is interesting to note that the plots of the A-jump data intersect that for the bulk diffusion of C in Fe between 1000 and 1200 K: this corresponds to the temperature range in which dissociation of C from an SIA cluster was observed in the MD simulations.

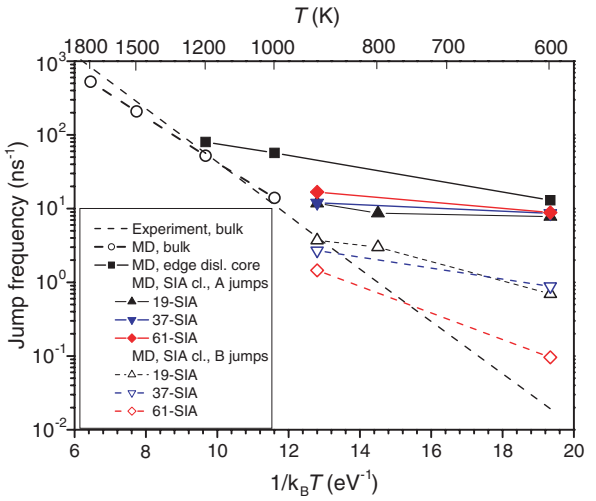

Fig. 6. Estimates of the jump frequency of a C atom in the core of the periphery of $\frac{1}{2}\langle 1\,1\,1\rangle$ 19-, 37- and 61-SIA clusters. Data are also included for the jump frequency of C atom in the core of a straight $\frac{1}{2}\langle 1\,1\,1\rangle$ edge dislocation obtained by MD simulation using the same Fe–C model as here (filled squares) [34] and for MD results [22] and experimental data [35,36] for C in the bulk of bcc iron.

Although the number of B-type jumps, in which the C solute migrates from one side of a cluster to another, obtainable by MD is small (see Table 2), it is clear that the ratio of B to A jump frequencies for the 19- and 37-SIA clusters increases with temperature, and that the number of B jumps observed is sufficient for an approximate analysis. (We exclude the 61-SIA defect from this because only small number of B migrations occurred at each temperature.) Within the uncertainty of the analysis, it is seen that the activation energy associated with the B jumps is 1.5–2 times higher than that for the A mechanism.

4.3. Implications for mobility of ⟨1 1 1⟩ SIA clusters

Several key results stand out from the preceding subsections. First, over the timescale possible in MD simulation, a C interstitial immobilises a cluster of seven SIAs at 300 K and dissociates from the cluster at 1200 K. At the intermediate temperatures considered (600 and 900 K), the cluster-C complex can co-migrate 1-D along the [1 1 1] direction of the crowdion axis. The length of the side of the 7-SIA defect is too short ($2a_0/\sqrt{6}$) for true dislocation core structure to develop, and this is the reason why this cluster exhibits 1-D motion, albeit with a much reduced jump frequency compared to that in pure iron.

Second, the larger clusters of 19, 37 and 61 SIAs modelled here trapped a C solute in their perimeter core at all temperatures except 1200 K when dissociation of the complex occurred. Although the C atom was able to jump in the core of the perimeter segments of the larger clusters at 600 and 900 K, the clusters were immobilised by the presence of C and were unable to diffuse along their [1 1 1] axis. This is explained by the fact that with increasing number of SIAs, cluster structure becomes more dislocation-like, with the result that C motion is only possible within the dislocation core [34]. The activation energy for this process approaches 0.2 eV as cluster size increases, which is the same as that for an infinite, straight edge dislocation (see Fig. 6). This is about a quarter of the value in the bulk crystal.

Third, although the dislocation core of a cluster provides an environment for rapid jumping of carbon at moderate temperature, it is significant that the vector of A-type jumps is $\pm\frac{1}{4}\langle 1\,1\,1\rangle$ at 70.5° to [1 1 1], and so is in neither the direction of $\boldsymbol{b}$ nor the ⟨1 1 2⟩ line direction of the core. When the C atom makes such a jump, the dislocation segment has to move by $\pm\frac{1}{12}[1\,1\,1]$ in order to retain the same C-cluster configuration. Thus, the SIA cluster can only move forward and backward by a small distance if a C interstitial stays trapped in the core of one side. Furthermore, if the C atom reaches a corner site by the cluster moving in, say, the [1 1 1] direction and then makes a B-type jump to an adjacent side, the only A steps available to it are those which force the cluster to move back in the reverse direction $[\bar{1}\bar{1}\bar{1}]$. This can be seen from the directions drawn on the glide prism faces in Fig. 5. Thus, although core migration of C around interstitial loops has been revealed here, the nature of the jump steps is such that only short back-and-forth displacements of the C-loop complex can occur. Carbon entrapment essentially immobilises the loops and long-range transport of carbon and loop is prevented.

5. Conclusions

(a) At 0 K, the most stable configuration of clusters containing less than five SIAs is $\frac{1}{2}\langle 1\,1\,0\rangle$, while the $\frac{1}{2}\langle 1\,1\,1\rangle$ configuration is preferable for larger clusters.
(b) At 0 K, rhombus-shaped $\frac{1}{2}\langle 1\,1\,0\rangle$ SIA clusters of about 16 SIAs and larger transform by the Eyre–Bullough mechanism [7] into ⟨1 0 0⟩ configuration, while retaining a habit plane between {1 1 0} and {1 0 0}.
(c) At 0 K, addition of two C atoms to a 9-SIA cluster makes ⟨1 0 0⟩ the most stable configuration, within the limitation of the model of non-interacting C atoms.
(d) In pure Fe, the dynamic behaviour of SIA clusters simulated here with a recent EAM-type potential [12] is similar to that obtained previously with a F–S-type potential [11]. In particular, independently of starting configuration, clusters with more than four SIAs transform into $\frac{1}{2}\langle 1\,1\,1\rangle$ configuration.
(e) At non-zero temperature, C atoms may form sessile complexes with clusters containing a few SIAs. Large clusters with one or two C atoms transform into $\frac{1}{2}\langle 1\,1\,1\rangle$-type configuration. Two C atoms may delay the transformation of ⟨1 0 0⟩ clusters or form sessile configurations.
(f) At non-zero temperature, there is no evidence of $\frac{1}{2}\langle 1\,1\,0\rangle$ to ⟨1 0 0⟩ transformation.
(g) C atoms captured by SIA clusters significantly reduce or prevent cluster mobility.
(h) C atoms migrate along the periphery of $\frac{1}{2}\langle 1\,1\,1\rangle$ clusters containing 19 or more SIAs with jump frequency similar to that for pipe diffusion along a straight edge dislocation.
(i) The C jump vector in (h) is the same as that in the core of a straight edge dislocation. As a result, long-range transport of carbon and loop is prevented.

Acknowledgements

K.T. would like to thank the Science Service Division of the Ministry of Science and Technology, Thailand, for providing a studentship grant. The

research was supported by a research grant from the UK Engineering and Physical Sciences Research Council; grant PERFECT (F160-CT-2003-508840) under programme EURATOM FP-6 of the European Commission; and partly by the Division of Materials Sciences and Engineering and the Office of Fusion Energy Sciences, US Department of Energy, under contract DE-AC05-00OR22725 with UT-Battelle, LLC.

References

[1] A.H. Cottrell, B.A. Bilby, Phys. Soc. London A 62 (1949) 49.
[2] A. Vehanen, P. Hautojarvi, J. Johansson, J. Yli-Kauppila, P. Moser, Phys. Rev. B 25 (1982) 762.
[3] E.A. Little, J. Nucl. Mater. 87 (1979) 11.
[4] E.A. Little, D.A. Stow, J. Nucl. Mater. 87 (1979) 25.
[5] B.L. Eyre, A.F. Bartlett, Philos. Mag. 12 (1965) 261.
[6] B.C. Masters, Philos. Mag. 11 (1965) 881.
[7] B.L. Eyre, R. Bullough, Philos. Mag. 12 (1965) 31.
[8] A.F. Calder, D.J. Bacon, J. Nucl. Mater. 207 (1993) 25.
[9] J. Marian, B.D. Wirth, Phys. Rev. Lett. 88 (2002) 255507.
[10] Yu.N. Osetsky, A. Serra, V. Priego, J. Nucl. Mater. 276 (2000) 202.
[11] G.J. Ackland, D.J. Bacon, A.F. Calder, T. Harry, Philos. Mag. A 75 (1997) 713.
[12] G.J. Ackland, M.I. Mendelev, D.J. Srolovitz, S. Han, A.V. Barashev, J. Phys.: Condens. Matter 16 (2004) S2629.
[13] F. Willaime, C.-C. Fu, M.C. Marinica, J. Dalla Torre, Nucl. Instrum. and Meth. B 228 (2005) 92.
[14] R.A. Johnson, G.J. Dienes, A.C. Damask, Acta Metall. 12 (1964) 1215.
[15] C.A. Wert, Phys. Rev. 79 (1950) 601.
[16] A.J. Bosman, P.E. Brommer, G.H. Rathenau, Physica 23 (1957) 1001.
[17] R.A. Arndt, A.C. Damask, Acta Metall. 12 (1964) 341.
[18] R.P. Smith, Trans. Metall. Soc. AIME 224 (1962) 105.
[19] G.K. Williamson, R.E. Smallmann, Acta Crystallogr. 6 (1953) 361.
[20] C. Domain, C.S. Becquart, J. Foct, Phys. Rev. B 69 (2004) 144112.
[21] W.B. Pearson, Lattice Spacings and Structures of Metals and Alloys, Pergamon, London, 1958, p. 919.
[22] K. Tapasa, A.V. Barashev, D.J. Bacon, Yu.N. Osetsky, Acta Mater. 55 (2007) 1.
[23] V. Rosato, Acta Metall. 37 (1989) 2759.
[24] M. Ruda, D. Farkas, J. Abriata, Scripta Mater. 46 (2002) 349.
[25] B.J. Lee, Acta Mater. 54 (2006) 701.
[26] S. Takaki, J. Fuss, H. Kugler, U. Dedek, H. Schults, Radiat. Eff. 79 (1983) 87.
[27] A.W. Cochardt, G. Schoek, H. Wiedersich, Acta Metall. 3 (1955) 533.
[28] J.T.M. de Hosson, Solid State Commun. 17 (1975) 747.
[29] D. Frenkel, B. Smit, Understanding Molecular Simulations: From Algorithms to Applications, Academic Press, San Diego, 1996.
[30] A.V. Barashev, Yu.N. Osetsky, D.J. Bacon, Philos. Mag. A 80 (2000) 2709.
[31] Yu.N. Osetsky, D.J. Bacon, A. Serra, B.N. Singh, S.I. Golubov, Philos. Mag. 83 (2003) 61.
[32] B.D. Wirth, G.R. Odette, D. Maroudas, G.E. Lucas, J. Nucl. Mater. 244 (1997) 185.
[33] Yu.N. Osetsky, A. Serra, B.N. Singh, S.I. Golubov, Philos. Mag. A 80 (2000) 2131.
[34] K. Tapasa, Yu.N. Osetsky, D.J. Bacon, Acta Mater. 55 (2007) 93.
[35] E.A. Brandes, Smithells Metals Reference Book, Butterworth, London, 1983.
[36] J.R.G. Da Silva, R.B. McLellan, Mater. Sci. Eng. 26 (1976) 83.